RESEARCH

Effect of real-time high temperature and loading rate on mode I fracture toughness of granite

Ke Yang[1], Fan Zhang[1]*, Fan-zhen Meng[2], Da-wei Hu[3] and Xian-feng Tan[4]

*Correspondence:
fanzhang@hbut.edu.cn

[1] School of Civil Engineering,
Architecture and Environment,
Hubei University of Technology,
Wuhan, China
[2] Qingdao University
of Technology, Qingdao, China
[3] State Key Laboratory
of Geomechanics
and Geotechnical Engineering,
Institute of Rock and Soil
Mechanics, Chinese Academy
of Sciences, Wuhan, China
[4] Faculty of Engineering, China
University of Geosciences,
Wuhan, China

Abstract

An in-depth understanding of the effect of real-time high temperature and loading rate on the fracture toughness of rocks is highly important for understanding the fracture mechanism of Hot Dry Rock (HDR). Three-point bending tests on notched semi-circular bending (NSCB) samples at the real-time temperatures (25, 100, 200, 300, 400 and 500 ℃) and different loading rates (0.1, 0.01 and 0.001 mm/min) were performed to characterize the temperature and rate dependence of the mode I fracture toughness. Besides, the characteristic of the fracture surface morphology was investigated by scanning electron microscope (SEM) and crack deviation distance analysis. Results show that the temperature has a significant effect on the development of intergranular and transgranular cracks. The fracture toughness and peak load are similarly influenced by temperature (i.e., they both decrease with increasing temperature). At the loading rates of 0.1 mm/min and 0.01 mm/min, from 25 to 400 °C, the fracture toughness decreases slightly with decreasing loading rates. However, at a loading rate of 0.001 mm/min, the fracture toughness values above 200 °C are very similar, and the fracture toughness does not strictly follow the law of decreasing with decreasing loading rate. Especially at 500 °C, fracture toughness and loading rate are negatively correlated. Our study also indicates that the effect of loading rate on macroscopic crack propagation path at real-time high temperature is not obvious. This study could provide an important basis for evaluating the safety and stability of geothermal engineering.

Keywords: Granite, Real-time high temperature, Loading rate, Fracture toughness, Notched semi-circular bending

Introduction

Hot dry rock (HDR) is recognized as a clean and renewable geothermal energy source (Tester et al. 2007). Under natural conditions, HDR with granite as the main rock type, the temperatures at a depth of 5 to 6 km are between 150 °C and 500 °C (Breede et al. 2013). When rock is exposed to high temperatures for long periods of time, the temperature can deteriorate the strength and structure of rock by the generation of thermal cracks (Feng et al. 2017). Tensile/opening (mode I) fracture is the main fracture mechanism in rock fracture processes (Dai et al. 2015), and the mode I fracture toughness is

Yang *et al. Geothermal Energy*   (2022) 10:14

Page 2 of 16

a critical parameter to evaluate the ability of rock to resist crack propagation (Bahrami et al. 2020). Therefore, a comprehensive understanding of the variation in mode I fracture toughness of granite at different temperatures is important for the design, construction and maintenance of geothermal engineering facilities.

To measure the mode I fracture toughness of rocks, four methods, namely, chevron-notched bend (CB) test and short rod (SR) test (Franklin et al. 1988), cracked chevron-notched Brazilian disk (CCNBD) test (Fowell et al. 1995) and semi-circular bend (SCB) test (Chong and Kuruppu 1984) have been proposed by the International Society for Rock Mechanics (ISRM). Different test methods have been performed to compare the obtained value of the mode I fracture toughness of different rocks (Dai et al. 2015; Wong et al. 2019). Among these methods, the SCB sample, also called notched semi-circular bending (NSCB) sample, has been widely used in rock mechanic community due to its advantage in the sample preparation and testing procedures (Kataoka et al. 2015). Wei et al. (2018) also summarized the above methods and proposed a novel chevron notched short rod bend method (CNSRB) to measure the mode I fracture toughness of rock. Moreover, the fracture behaviour of NSCB sample is more consistent with the hypothesis of the theoretical fracture mechanism (Dai et al. 2015). Therefore, NSCB sample was selected for fracture toughness measurement in this study.

High temperatures not only affect the physical properties of the rock (e.g., porosity, wave velocity and permeability), but also influence the mechanical behavior (compressive strength and elastic modulus) (Zhang et al. 2018; Zhao et al. 2020; Meng et al. 2021). A number of studies have been performed to investigate the effect of high temperature treatment on the fracture toughness of rocks (i.e., the rock is first heated to the target temperature, and then cooled to room temperature, and the test was then performed on the thermally treated specimens at room temperature). For example, the fracture toughness of sandstone was found to first increase and then decrease with the increasing of thermal treatment temperature, which were considered to be closely associated with the closure of previous cracks and the development of thermal cracks (Feng et al. 2017; Mahanta et al. 2016; Zuo et al. 2014). The fracture toughness of granite gradually decreased with the increase of thermal treatment temperature, which was thought to be caused by the development of thermal cracks and quartz phase transformation (Meredith and Atkinson 1985; Yin et al. 2012; Yin et al. 2019; Yin et al. 2020; Zuo et al. 2017). In the study of Yin et al. (2018), however, the authors found that fracture toughness values of granite were similar between 100 °C and 200 °C, and between 400 °C and 600 °C, and the former was caused by the improved sample mass densities as a result of mineral expansion, while the latter was related to the fact that the temperature did not further aggravate the thermal damage of the granite.

At present, most of the studies on the temperature dependence of the fracture toughness of granite have been performed on rocks after thermal treatment. The thermal treatment tests are inadequate to represent the fracture toughness variation of rocks in actual geothermal engineering, and the effects of different real-time temperature on the mode I fracture mode, fracturing mechanism and fracture toughness remain elusive. In addition, the rate of water injection is also an important factor affecting geothermal extraction. Different injection rates may affect the initiation and propagation of fractures, thus influencing the scale of fracture network and heat transfer efficiency (Zhuang

Yang *et al. Geothermal Energy*   (2022) 10:14

Page 3 of 16

et al. 2019). Studying the loading rate effects of the fracturing mechanism at different real-time temperatures can help to optimize the injection rate of fracturing. A number of previous laboratory tests have been performed to analyze the effects of loading rate on the static fracture toughness of different rocks. However, no consensus has been obtained. For example, the static fracture toughness of limestone was found to decrease slightly with decreasing loading rate (Bažant et al. 1993), while the static fracture toughness of sandstone was found to be independent on the loading rate (Backers et al. 2003). How the fracture toughness and fracture mode are affected by the coupled effects of different real-time temperatures and loading rates needs more in-depth study.

In this work, three-point bending tests were conducted on NSCB samples at different real-time temperatures (e.g., 25, 100, 200, 300, 400 and 500 °C) and three loading rates (e.g., 0.1, 0.01 and 0.001 mm/min), the mode I fracture toughness at real-time temperature was obtained and then compared with that obtained in the rapid water-cooling test after thermal treatment. The effect of the loading rate on the mode I fracture toughness was also analysed.

Experiment procedure

Sample preparation

The granite used in the tests was sampled from Shuitou Town, Fujian Province, China. Its natural density and porosity are 2.76 g/cm^3 and 0.62%, respectively. Analysis of the mineral composition by X-ray diffraction (XRD) shows that the main mineral compositions and average mass fractions of the granite are albite (39.63%), biotite (39.15%), quartz (16.76%), and tremolite (4.46%). As shown in Fig. 1, the geometry and size of samples were processed in accordance with the standard of ISRM (Kuruppu et al. 2014). All samples were drilled from the same batch of granite blocks with 76 mm diameter cores. The cores were then cut into NSCB samples and the flatness of each end surface was polished according to the suggested method (Kuruppu et al. 2014).

Experimental equipment

A universal testing machine (Fig. 2a) was used to perform the three-point bending test on the NSCB samples. The maximum loading force of the testing machine is 300 kN, and the resolution of the test force is 1/500000. The maximum temperature of the high temperature control box (Fig. 2b) is 500 °C, and the three-point bending fixture is rigid enough to resist the high temperature during the test. During the loading tests, the applied load was measured by the pressure sensor and the displacement
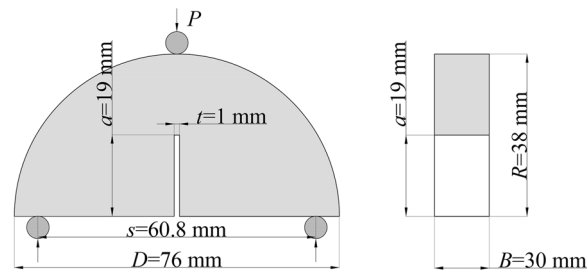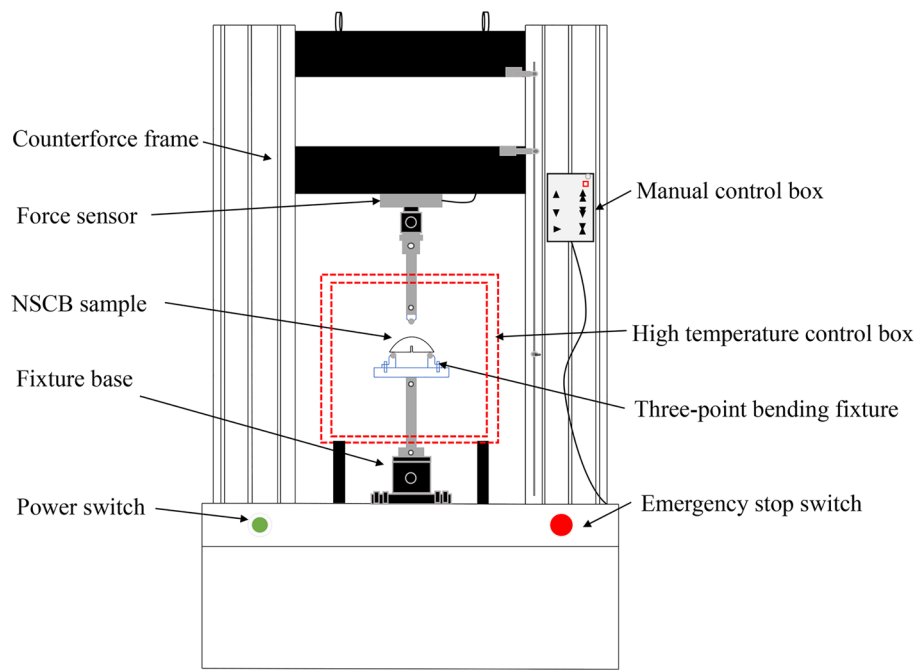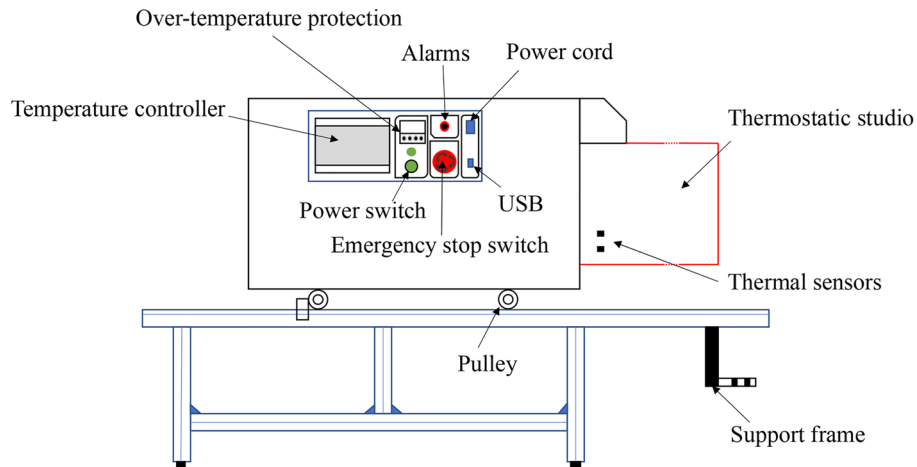

Fig. 1 NSCB sample size

(a) Universal testing machine

(b) High temperature control box

Fig. 2 Experimental equipment **a** universal testing machine **b** High temperature control box

was recorded by the loading system. The samples were first placed symmetrically on the three-point bending fixture, then the temperature was raised at a heating rate of 10 °C/min until the target temperature was reached. The target temperature was kept at least for 2 h in the high temperature control box to ensure uniform temperature distribution inside of the rock sample (Yin et al. 2019; Zhang et al. 2018). The loading indenter was lowered at the designed loading rate (i.e., 0.1, 0.01 and 0.001 mm/min)

until the sample fractured. More than 3 samples were tested for each set of condition, and the average value was taken for the results analysis.

To evaluate the stability of the test equipment, we tested 5 NSCB samples at 100 °C and a loading rate of 0.01 mm/min, and the load–displacement curves are given in Fig. 3. The shape of the load–displacement curve at the same initial boundary conditions are similar for multiple samples tested, indicating that the performance of the equipment is reliable.

Analysis of the test results

Load–displacement curve analysis

Figure 4 shows the load–displacement curves obtained for the granite NSCB samples in the three-point bending tests. The curve usually consists of compaction stage, linear elastic stage and failure stage. During the compaction stage, the slope of the curve increases nonlinearly. After reaching the linear elastic stage, the load increases linearly with the displacement increases. Below 300 °C, the load drops abruptly after the peak and the sample fails drastically, exhibiting a typical brittle fracture. At 400 °C, the load–displacement curves at larger loading rates (0.1 mm/min and 0.01 mm/min) fluctuate before reaching the peak load (Fig. 4a, b), and the decreasing trend becomes slower in the failure stage (Fig. 4a). These phenomena may be caused by the decreasing brittleness of the samples under high temperature. It is worth noting that at a loading rate of 0.001 mm/min, the curve at 300 °C has fluctuated before the peak, and the failure stage at 400 °C begins to show progressive rupture characteristics (Fig. 4c). This indicates that at lower loading rates (0.001 mm/min), the brittleness of the samples begins to weaken at lower temperatures. When the temperature rises to 500 °C (Fig. 4a, b, c), the curves are generally jagged at the failure stage, and the sample progressively ruptured until complete failure. The samples still have the ability to resist the external load when they are damaged, which is related to the decreasing brittleness of the rock with increasing temperature.

At the loading rate of 0.1 and 0.01 mm/min, there is no obvious difference in the compaction stage of the curve, and the failure displacement basically increases with the
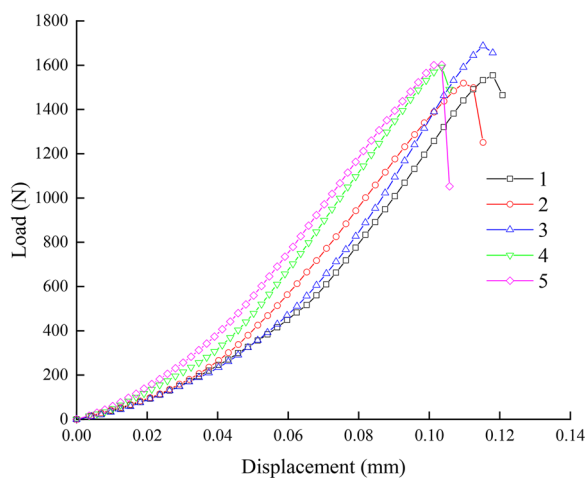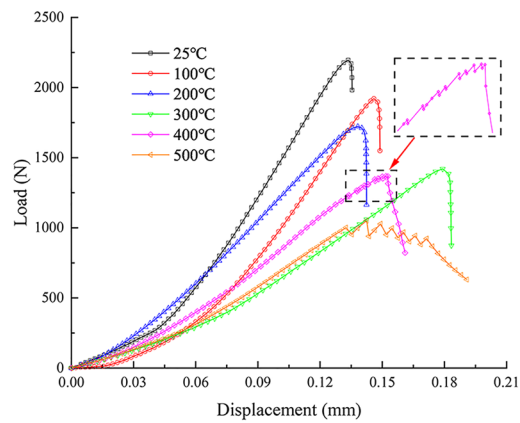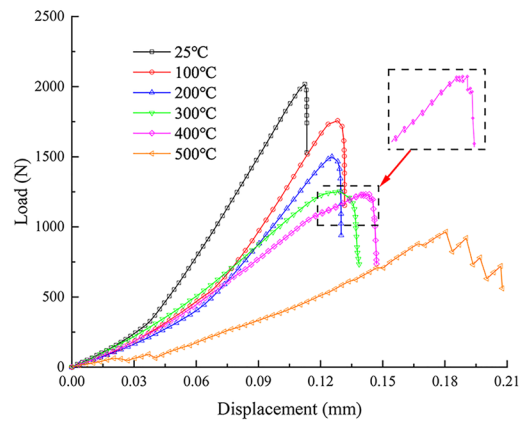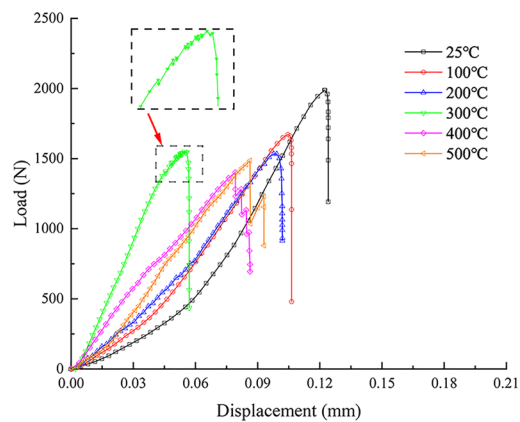

Fig. 3 Example of load–displacement curve (100 °C and 0.01 mm/min)

(a) 0.1 mm/min loading rate

(b) 0.01 mm/min loading rate

(c) 0.001 mm/min loading rate

Fig. 4 Load–displacement curves at different temperatures and loading rates. **a** 0.1 mm/min loading rate. **b** 0.01 mm/min loading rate. **c** 0.001 mm/min loading rate

increase of temperature. When the loading rate is reduced to 0.001 mm/min, the compaction stage is almost invisible above 200 ℃, and the failure displacement decreases first and then increases with increasing temperature. In addition, at the three loading rates, the failure displacement generally increases with increasing loading rate. The

above comparison shows that not only the high temperature, but also the loading rate affects the mechanical behaviour of granite.

As shown in Fig. 5, the peak load decreases generally with increasing temperature at all three loading rates, which is related to the damage of granite caused by high temperature. However, the loading rate poses different influence on the peak load at low and high temperatures. Below 200 ℃, the peak load increases with the increase of loading rate. From 200 °C to 400 °C, the peak loads at loading rates of 0.1 mm/min and 0.01 mm/min are still positively related to the loading rate. However, at a loading rate of 0.001 mm/min, the peak load is the largest. Especially at 500 ℃, the peak load decreases with the increase of loading rate, which indicates that the high temperature reverses the loading rate effect on the peak loading.

Fracture toughness analysis

The mode I fracture toughness K_{IC} of NSCB samples is calculated according to the following formula given by ISRM (Kuruppu et al. 2014):

$$K_{IC} = Y' \frac{P_{max}\sqrt{\pi a}}{2RB} \tag{1}$$

$$Y' = -1.297 + 9.516(\frac{s}{2R}) - (0.47 + 16.457(\frac{s}{2R}))\beta + (1.071 + 34.401(\frac{s}{2R}))\beta^2 \tag{2}$$

where Y' is the non-dimensional stress intensity factor; P_{max} is the maximum load at sample failure; R, a and B are the production dimensions of the samples; s is the support span, $s/2R = 0.8$; β is the normalized length, $\beta = a/R = 0.5$.

According to the above Eqs. (1, 2), the fracture toughness was calculated for different real-time temperatures and loading rates. The average fracture toughness and standard deviation are illustrated in Table 1. Compared with the fracture toughness at 25 °C, when the temperature increases from 100 to 500 °C, the fracture toughness at the loading rate of 0.1 mm/min decreases by 13.22%, 22.21%, 32.25%, 34.50%
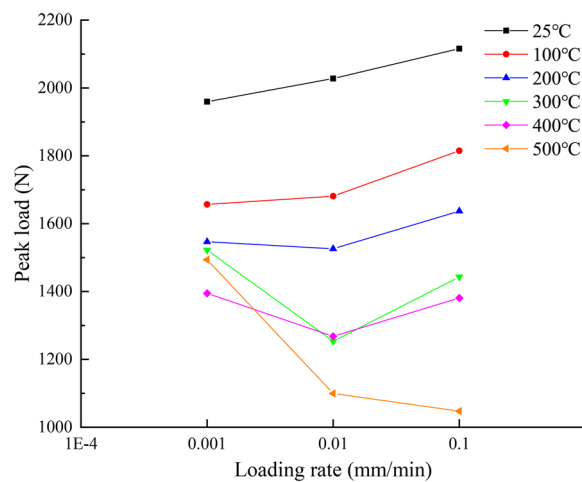

Fig. 5 Peak load versus loading rate at different temperatures

Table 1 Results of the fracture toughness

temperature (℃)	Loading rate (mm/min)	Average fracture toughness (MPa·m$^{1/2}$)	Standard deviation (MPa·m$^{1/2}$)
25	0.1	1.513	0.070
	0.01	1.449	0.015
	0.001	1.420	0.029
100	0.1	1.313	0.102
	0.01	1.220	0.037
	0.001	1.191	0.069
200	0.1	1.177	0.058
	0.01	1.095	0.056
	0.001	1.113	0.101
300	0.1	1.025	0.104
	0.01	0.908	0.063
	0.001	1.094	0.038
400	0.1	0.991	0.016
	0.01	0.906	0.072
	0.001	1.002	0.017
500	0.1	0.755	0.018
	0.01	0.792	0.089
	0.001	1.074	0.023

$$K_{IC(0.1)}=-0.10119+1.63492\times e^{(T/-837.08347)}$$
$$R^2=0.97036$$

$$K_{IC(0.001)}=1.05077+0.4888\times e^{(T/-86.40703)}$$
$$R^2=0.95775$$

$$K_{IC(0.01)}=0.70896+0.81018\times e^{(T/-242.50761)}$$
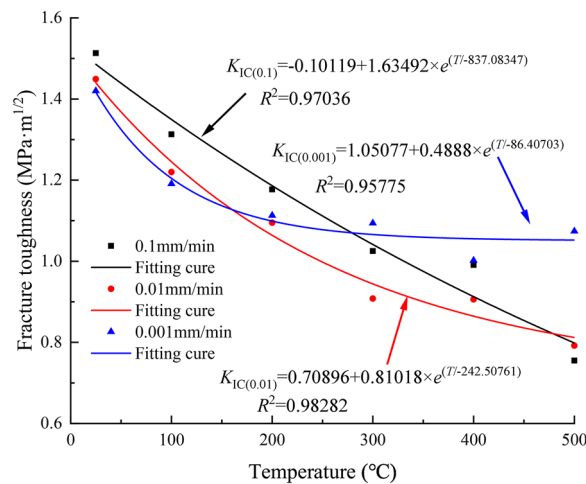$$R^2=0.98282$$

Fig. 6 Fracture toughness versus real-time high temperature

and 50.10%, respectively; the fracture toughness at the loading rate of 0.01 mm/min decreases by 15.80%, 24.43%, 37.34%, 37.47% and 45.34%, respectively; and the fracture toughness at the loading rate of 0.001 mm/min decreases by 16.13%, 21.62%, 22.96%, 29.44% and 24.37, respectively. The high temperature obviously reduces the fracture toughness of granite.

Figure 6 shows the trend of granite fracture toughness with real-time high temperature. Exponential function is used to fit the variation of the average fracture toughness with temperature, and the following fitting equations are obtained:

$$K_{\mathrm{IC}(0.1)} = -0.10119 + 1.63492 \times e^{(T/(-837.08347))}$$
$$R^2 = 0.97036 \tag{3}$$

$$K_{\mathrm{IC}(0.01)} = 0.70896 + 0.81018 \times e^{(T/(-242.50761))}$$
$$R^2 = 0.98282 \tag{4}$$

$$K_{\mathrm{IC}(0.001)} = 1.05077 + 0.4888 \times e^{(T/-86.40703)}$$
$$R^2 = 0.95775 \tag{5}$$

where $K_{\mathrm{IC}(0.1)}, K_{\mathrm{IC}(0.01)}$ and $K_{\mathrm{IC}(0.001)}$ represent the fracture toughness at different loading rates, T represents temperature, R^2 represents the correlation coefficient.

From 25 to 400 °C, the fracture toughness at the loading rate of 0.1 mm/min is greater than that at the loading rate of 0.01 mm/min. The increase of loading rate has a certain toughening effect on granite, but this strengthening effect is not obvious, and the difference of fracture toughness between the two is within 0.117 MPa·m$^{1/2}$. It is worth noting that at the loading rate of 0.001 mm/min, the fracture toughness is not significantly affected by temperature above 200 °C, decreasing by only 0.039 MPa·m$^{1/2}$ from 200 to 500 °C. The fracture toughness does not strictly follow a monotonic decrease with temperature, which may be caused by the inhomogeneity of the granite material (Yin et al. 2018). It can also be seen that the variation law of fracture toughness and peak load with real-time temperature or loading rate is consistent, indicating that the fracture toughness is proportional to peak load.

Macro-fracture traces analysis

The NSCB samples after tests are shown in Fig. 7, which clearly shows that the colour of the samples changed from blue–grey below 300 ℃ to slightly yellow at 400 ℃. At 500 ℃, the samples turn to be beige in colour and some debris can be observed at the notch of prefabricated crack. The phenomenon is attributed to that the biotite-rich granite turns to be yellow in colour at high temperature (Vazquez et al. 2016). Figure 8 shows the traces of the fracture plane, which initiates from the middle of the straight notch and then propagates along the axial direction.
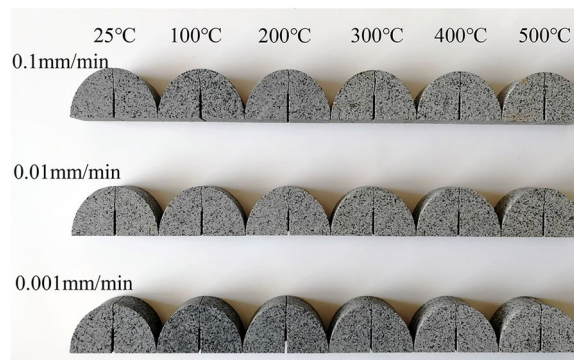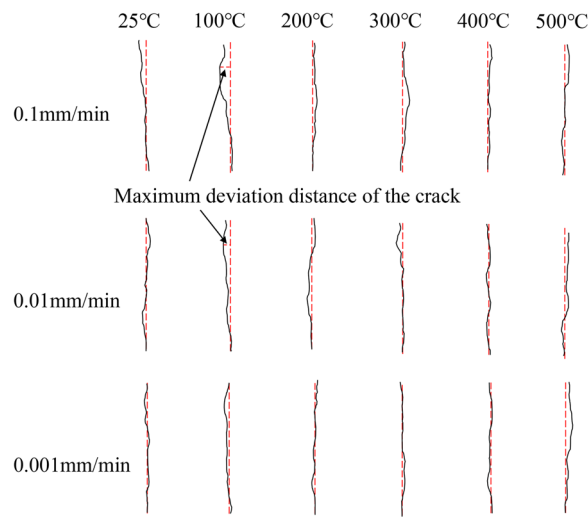

Fig. 7 NSCB samples after testing

Yang *et al. Geothermal Energy*   (2022) 10:14

Page 10 of 16

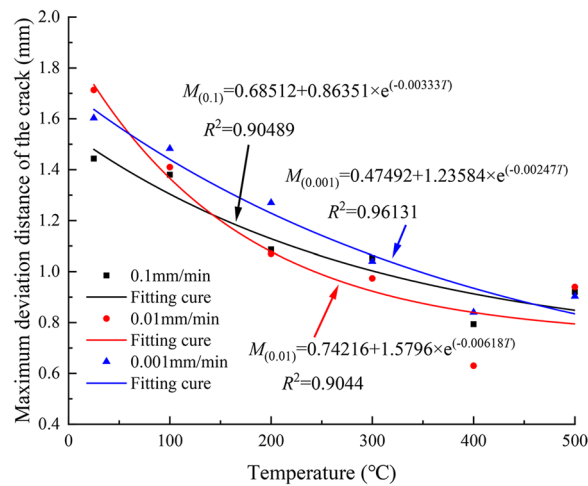**Fig. 8** Macro-fracture traces

Fig. 9 Maximum deviation distance of the crack at different temperatures

The maximum deviation distance of the crack (Fig. 8) is defined as the perpendicular distance from the crack to the center line of the prefabricated straight notch plane (Wong et al. 2019). As shown in Fig. 9, temperature has a significant effect on the maximum deviation distance, and the temperature reduces the deviation distance of the cracks. The reason is that the high temperature reduces the strength of the rock, and cracks are more likely to expand axially along the prefabricated straight notch under load (Feng et al. 2017). Based on the research of Kuruppu et al. (2014), the maximum deviation distance of the crack should be less than 0.05D, otherwise the sample is subjected to the torsion and shear (i.e., I–II mixed mode fracture occurs). Our test results in Fig. 9 shows that the maximum deviation distance of the crack is 1.71 mm, indicating that pure tensile failure occurs. The maximum deviation distance of the cracks is close to each other for NSCB samples under different loading rates, indicating the loading rate

has insignificant effect on the deviation degree of the crack. Exponential function is used to fit the variation of the maximum crack deviation distance with temperature, and the following results are obtained:

$$M_{(0.1)} = 0.68512 + 0.86351 \times e^{(-0.00333T)}$$
$$R^2 = 0.90489 \tag{6}$$

$$M_{(0.01)} = 0.74216 + 1.5796 \times e^{(-0.00618T)}$$
$$R^2 = 0.9044 \tag{7}$$

$$M_{(0.001)} = 0.47492 + 1.23584 \times e^{(-0.00247T)}$$
$$R^2 = 0.96131 \tag{8}$$

where $M_{(0.1)}, M_{(0.01)}$ and $M_{(0.001)}$ is the maximum deviation distance of the crack at different loading rates.

Micro-damage analysis

Moreover, micro-damages on the fracture surface were also observed by SEM from the microscopic scale. The images of microcracks are shown in Fig. 10, where the number of micro cracks in granite obviously increases with temperature. The main mineral components of the granite in this study are albite, quartz and biotite. At 25 ℃, the micro-structure of the granite is comparatively intact. The pre-existing cracks and weak boundaries between mineral grains in granite are locally damaged when the material is stressed, resulting in a small number of cracks. From 25 ℃ to 300 ℃, the number of microcracks begins to increase, and the aperture of the cracks also tends to increase (Fig. 10a–d). They are mainly intergranular cracks, which occur in quartz particles, feldspar particles,
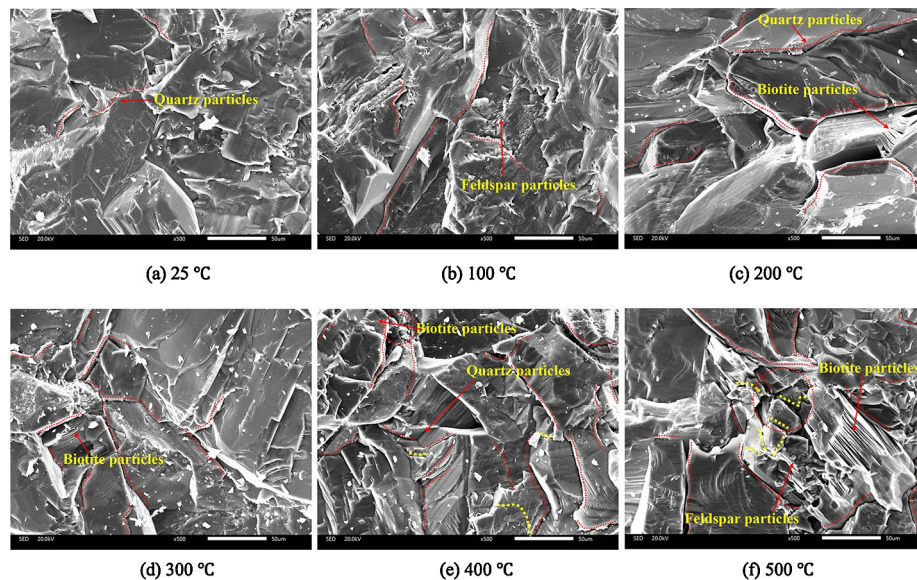

Fig. 10 SEM images of granite at 25–500 ℃ and 0.01 mm/min loading rate (The red lines indicate the intergranular cracks, the yellow lines indicate the transgranular cracks, and the red circles indicate the broken area.). **a** 25 ℃. **b** 100 ℃. **c** 200 ℃. **d** 300 ℃. **e** 400 ℃. **f** 500 ℃

or between quartz and feldspar particles (Yang. 2022). The main reason for the formation of microcracks at high temperatures is that the granite is composed of mineral particles with different thermal expansion coefficients and thermoelastic coefficients, and the mineral particles produce uneven expansion at high temperatures (Sun et al. 2015). At 400 °C, the number of intergranular cracks increases sharply and transgranular cracks begin to appear (Fig. 10e). When the temperature is increased to 500 °C, a large number of transgranular cracks appear in the sample, and the intergranular cracks and transgranular cracks are interconnected to form a large broken area (Fig. 10f). Transgranular cracks mainly appear in feldspar particles, which is due to the lower strength of feldspar than quartz (Yang. 2022). Below 500 °C, intergranular cracks appear rarely between biotite particles. The reason is that the distinctive layered microstructure of biotite, which causes cracks to be generally hindered by biotite grains and to develop around their boundaries (Li et al. 2002).

Discussion

Influence of the high temperature and loading rate

Under the combined effect of real-time high temperature and mechanical loading, the number of microcracks increases gradually with temperature. The mechanical properties of granite at high temperatures can be understood with the assistance of microstructure evolutions. When the minerals cannot withstand the thermal stress caused by thermal expansion, high temperature can cause the thermal damage to granite, resulting in microcracks within the rock, which reduces the strength of the rock (Yang et al. 2017; Feng et al. 2017).

Since the fracture toughness is proportional to the peak load, the effect of loading rate is analyzed from the variation of fracture toughness. At the loading rates of 0.1 mm/min and 0.01 mm/min, from 25 to 400 °C, the fracture toughness decreases slightly with decreasing loading rate. At lower loading rates, the microcracks in the sample have enough time to evolve and develop, and more energy is consumed for microcrack propagation, resulting in less energy released when the sample fractures, which leads to the reduction of fracture toughness (Xie et al. 2020). When the loading rate is 0.001 mm/min, the fracture toughness values are similar above 200 °C, and the fracture toughness does not strictly follow the law of positive correlation with the loading rate. This is related to the fact that there is no obvious compaction stage in the load–displacement curve, and the compaction stage consumes almost no energy from the rock, resulting in a large fracture toughness value. It is mainly influenced by the coupling effect of real-time high temperature and low loading rate (0.001 mm/min), and also related to the anisotropy of granite mineral materials. In addition, when the temperature is 500 °C, the fracture toughness decreases with the increasing loading rate, and the effect of the loading rate is reversed by the temperature. This is related to a large number of transgranular cracks at 500 °C. The cracks at high loading rates are mostly transgranular cracks, which consume more energy than intergranular cracks (Yin et al. 2018). Therefore, at higher loading rates, transgranular cracks further weaken the mechanical properties of the rock, resulting in lower fracture toughness of the rock sample. Further research is needed to confirm this novel finding.

Influence of the heat treatment

As shown in Fig. 11, the real-time high temperature test is compared with the rapid water-cooling test after thermal treatment. The granite samples, processing dimensions, test equipment and loading rates are the same for both studies. The granite samples in the rapid water-cooling test were heated and kept for 2 h in a high-temperature muffle furnace, and cooled immediately to room temperature in normal temperature water, and then tested at room temperature (Lv. 2022). The result shows that the fracture toughness in both studies decreases with increasing temperature. At 25 °C, the deviation of fracture toughness (0.082 MPa·m$^{1/2}$) is caused by the anisotropy of the granite samples. At real-time high temperature, the fracture toughness decreases sharply from 25 to 100 °C, which is due to the fracture of the initial weak boundary of the particles in the sample, indicating that the fracture toughness is sensitive to temperature. Compared with real-time high temperature, the fracture toughness of water-cooled treatment increases slightly between 100 °C and 200 °C. The reason is that the high temperature gradient due to rapid water-cooling will cause thermal hardening, which induces strong cooling-related shrinkage of the sample, the denseness inside the sample is increased and the strength of the rock is enhanced (Zhang et al. 2020). Thermal hardening increases the fracture toughness of the samples. From 200 to 500 °C, the fracture toughness at real-time high temperatures is reduced by only 7%. The fracture toughness of water-cooled treatments continued to decrease rapidly above 200 °C. The reason is that the thermal shock caused by rapid water-cooling leads to significant extension of microcracks, and water-induced mineral dissolution also weakens the overall properties of the rock (Yin et al. 2019). The damage caused by rapid water-cooling dominates, and the fracture toughness of the samples are drastically reduced. From 300 to 400 °C, the fracture toughness decreases in the real-time high temperature and water-cooled treatment tests are only 3.32% and 0.22%, respectively. The reason is that the ductility of biotite particles in granite is strengthened at high temperature, which slows down the decrease of the mechanical properties of the samples (Ma et al. 2020).
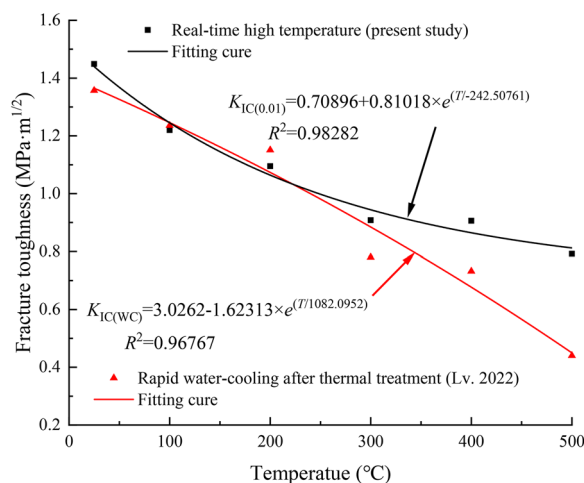

Fig. 11 Fracture toughness under different test conditions

The relation between fracture toughness and temperature under rapid water-cooling is fitted as follows:

$$K_{\mathrm{IC(WC)}} = 3.0262 - 1.62313 \times e^{(T/1082.0952)}$$
$$R^2 = 0.96767$$

(9)

where $K_{\mathrm{IC(WC)}}$ is fracture toughness under rapid water-cooling test.

Conclusions

In this study, the three bending tests by NSCB method were conducted at real-time temperature (25, 100, 200, 300, 400 and 500 ℃) and different loading rates (0.1, 0.01 and 0.001 mm/min). The mode I fracture toughness and fracture characteristics of the granite were analyzed from the initiation and development of the microcracks. At real-time high temperature, the fracture toughness is proportional to the peak load. The number of microcracks increases significantly with temperature, leading to a decrease in fracture toughness with increasing temperature. Compared with the rapid water-cooling test after thermal treatment, the real-time high temperature above 200 ℃ has less damage to the mechanical properties of granite. When the loading rate is 0.1 mm/min and 0.01 mm/min, the fracture toughness decreases slightly with decreasing loading rate from 25 to 400 ℃. At the loading rate of 0.001 mm/min, from 200 ℃ to 500 ℃, the fracture toughness does not strictly follow the law of decrease with decreasing loading rate, and the variation of fracture toughness with temperature does not strictly follow the law of monotonic decrease. Fracture toughness and loading rate are negatively correlated at 500 ℃, indicating that the high temperature reverses the effect of loading rate. In addition, the effect of loading rate on the maximum deviation distance of macroscopic cracks is also not obvious.

Declarations

Competing interests
There is no dispute of interest with others.

References

Backers T, Fardin N, Dresen G, Stephansson O. Effect of loading rate on Mode I fracture toughness, roughness and micromechanics of sandstone. Int J Rock Mech Min Sci. 2003;40:425–33. https://doi.org/10.1016/S1365-1609(03)00015-7.

Bahrami B, Ayatollahi MR, Mirzaei AM, Yazid YM. Support type influence on rock fracture toughness measurement using semi-circular bending specimen. Rock Mech Rock Eng. 2020;53:2175–83. https://doi.org/10.1007/s00603-019-02023-z.

Bažant ZP, Bai SP, Gettu R. Fracture of rock: effect of loading rate. Eng Fract Mech. 1993;45(3):393–8. https://doi.org/10.1016/0013-7944(93)90024-M.

Breede K, Dzebisashvili K, Liu XL, Falcone G. A systematic review of enhanced (or engineered) geothermal systems: past, present and future. Geotherm Energy. 2013;1:4. https://doi.org/10.1186/2195-9706-1-4.

Chong KP, Kuruppu MD. New specimen for fracture toughness determination for rock and other materials. Int J Fract. 1984;26(2):R59–62. https://doi.org/10.1007/BF01157555.

Dai F, Wei MD, Xu NW, Zhao T, Xu Y. Numerical investigation of the progressive fracture mechanisms of four ISRM-suggested specimens for determining the mode I fracture toughness of rocks. Comput Geotech. 2015;69:424–41. https://doi.org/10.1016/j.compgeo.2015.06.011.

Feng G, Kang Y, Meng T, Hu YQ, Li XH. The influence of temperature on mode I fracture toughness and fracture characteristics of sandstone. Rock Mech Rock Eng. 2017;50(8):2007–19. https://doi.org/10.1007/s00603-017-1226-y.

Fowell RJ, Hudson JA, Xu C, Chen JF, Zhao X. Suggested method for determining mode I fracture toughness using cracked chevron notched brazilian disc (CCNBD) specimens. Int J Rock Mech Min Sci Geomech Abstr. 1995;32(7):322. https://doi.org/10.1016/0148-9062(95)92395-X.

Franklin JA, Sun ZQ, Atkinson BK, et al. Suggested methods for determining the fracture toughness of rock. Int J Rock Mech Min Sci Geomech Abstr. 1988;25(2):71–96. https://doi.org/10.1016/0148-9062(88)91871-2.

Kataoka M, Obara Y, Kuruppu M. Estimation of fracture toughness of anisotropic rocks by Semi-Circular Bend (SCB) tests under water vapor pressure. Rock Mech Rock Eng. 2015;48:1353–67. https://doi.org/10.1007/s00603-014-0665-y.

Kuruppu MD, Obara Y, Aytollahi MR, Chong KP, Funatsu T. ISRM-Suggested method for determining the mode I static fracture toughness using Semi-Circular bend specimen. Rock Mech Rock Eng. 2014;47:267–74. https://doi.org/10.1007/s00603-013-0422-7.

Li L, Tsui Y, Lee PKK, Tham LG, Li TJ, Ge XR. Progressive cracking of granite plate under uniaxial compression. Chin J Rock Mech Eng. 2002;21(7):940–7.

Lv DB. Experimental study on three point bending of granite after high temperature heat treatment. HuBei University of Technology. 2022.

Ma X, Wang GL, Hu DW, Liu YG, Zhou H, Liu F. Mechanical properties of granite under real-time high temperature and three-dimensional stress. Int J Rock Mech Min Sci. 2020;136: 104521. https://doi.org/10.1016/j.ijrmms.2020.104521.

Mahanta B, Singh TN, Ranjith PG. Influence of thermal treatment on mode I fracture toughness of certain Indian rocks. Eng Geol. 2016;210:103–14. https://doi.org/10.1016/j.enggeo.2016.06.008.

Meng FZ, Song J, Wong LNY, Wang ZQ, Zhang CQ. Characterization of roughness and shear behavior of thermally treated granite fractures. Eng Geol. 2021;293: 106287. https://doi.org/10.1016/j.enggeo.2021.106287.

Meredith PG, Atkinson BK. Fracture toughness and subcritical crack growth during high-temperature tensile deformation of Westerly granite and Black gabbro. Phys Earth Planet Inter. 1985;39(1):33–51. https://doi.org/10.1016/0031-9201(85)90113-X.

Sun Q, Zhang WQ, Xue L, Zhang ZZ, Su TM. Thermal damage pattern and thresholds of granite. Environ Earth Sci. 2015;74(3):2341–9. https://doi.org/10.1007/s12665-015-4234-9.

Tester JW, Anderson BJ, Batchelor AS, et al. Impact of enhanced geothermal systems on US energy supply in the twenty-first century. Phil Trans R Soc. 2007;365:1057–94. https://doi.org/10.1098/rsta.2006.1964.

Vazquez P, Acuña M, Benavente D, Gibeaux S, Navarro I, Gomez-Heras M. Evolution of surface properties of ornamental granitoids exposed to high temperatures. Constr Build Mater. 2016;104:263–75. https://doi.org/10.1016/j.conbuildmat.2015.12.051.

Wei DM, Dai F, Xu NW, Liu Y, Zhao T. A novel chevron notched short rod bend method for measuring the mode I fracture toughness of rocks. Eng Fract Mech. 2018;190:1–15. https://doi.org/10.1016/j.engfracmech.2017.11.041.

Wong LNY, Guo TY, Lam WK, Ng JYH. Experimental study of cracking characteristics of Kowloon granite based on three mode I fracture toughness methods. Rock Mech Rock Eng. 2019;52:4217–35. https://doi.org/10.1007/s00603-019-01882-w.

Xie Q, Li SX, Liu XL, Gong FQ, Li XB. Effect of loading rate on fracture behaviors of shale under mode I loading. J Cent South Univ. 2020;27:3118–32. https://doi.org/10.1007/s11771-020-4533-5.

Yang SQ. Thermal damage and failure mechanical behavior of granite after exposure to different high temperature treatments under uniaxial compression. In: Yang SQ, editor. Mechanical behavior and damage fracture mechanism of deep rocks. Singapore: Springer; 2022. p. 345–72.

Yang SQ, Ranjith PG, Jing HW, Tian WL, Ju Y. An experimental investigation on thermal damage and failure mechanical behavior of granite after exposure to different high temperature treatments. Geothermics. 2017;65:180–97. https://doi.org/10.1016/j.geothermics.2016.09.008.

Yang *et al. Geothermal Energy*   (2022) 10:14

Page 16 of 16

Yin TB, Li XB, Xia KW, Huang S. Effect of thermal treatment on the dynamic fracture toughness of Laurentian granite. Rock Mech Rock Eng. 2012;45(6):1087–94. https://doi.org/10.1007/s00603-012-0240-3.

Yin TB, Bai L, Li X, Li XB, Zhang SS. Effect of thermal treatment on the mode I fracture toughness of granite under dynamic and static coupling load. Eng Fract Mech. 2018;199:143–58. https://doi.org/10.1016/j.engfracmech.2018.05.035.

Yin TB, Li Q, Li XB. Experimental investigation on mode I fracture characteristics of granite after cyclic heating and cooling treatments. Eng Fract Mech. 2019;222: 106740. https://doi.org/10.1016/j.engfracmech.2019.106740.

Yin TB, Wu Y, Li Q, Wang C, Wu BQ. Determination of double-K fracture toughness parameters of thermally treated granite using notched semi-circular bending specimen. Eng Fract Mech. 2020;226: 106865. https://doi.org/10.1016/j.engfracmech.2019.106865.

Zhang F, Zhao JJ, Hu DW, Skoczylas F, Shao JF. Laboratory investigation on physical and mechanical properties of granite after heating and water-cooling treatment. Rock Mech Rock Eng. 2018;51(3):677–94. https://doi.org/10.1007/s00603-017-1350-8.

Zhang F, Zhang YH, Yu YD, Hu DW, Shao JF. Influence of cooling rate on thermal degradation of physical and mechanical properties of granite. Int J Rock Mech Min Sci. 2020;129: 104285. https://doi.org/10.1016/j.ijrmms.2020.104285.

Zhao ZH, Xu HR, Wang J, Zhao XG, Cai M, Yang Q. Auxetic behavior of Beishan granite after thermal treatment: a microcracking perspective. Eng Fract Mech. 2020;231: 107017.

Zhuang L, Kim KY, Jung SG, Diaz M, Min KB. Effect of water infiltration, injection rate and anisotropy on hydraulic fracturing behavior of granite. Rock Mech Rock Eng. 2019;52:575–89. https://doi.org/10.1007/s00603-018-1431-3.

Zuo JP, Xie HP, Dai F, Yang J. Three-point bending test investigation of the fracture behavior of siltstone after thermal treatment. Int J Rock Mech Min Sci. 2014;70:133–43. https://doi.org/10.1016/j.ijrmms.2014.04.005.

Zuo JP, Wang JT, Sun YJ, Chen Y, Jiang GH, Li YH. Effects of thermal treatment on fracture characteristics of granite from Beishan, a possible high-level radioactive waste disposal site in China. Eng Fract Mech. 2017;182:425–37. https://doi.org/10.1016/j.engfracmech.2017.04.043.

Publisher's Note